AD-A084 410 MASSACHUSETTS INST OF TECH LEXINGTON LINCOLN LAB F/G 9/3
ELECTROOPTICAL DEVICES.(U)
SEP 79 C E HURWITZ F19628-80-C-0002
UNCLASSIFIED ESD -TR-79-279 NL

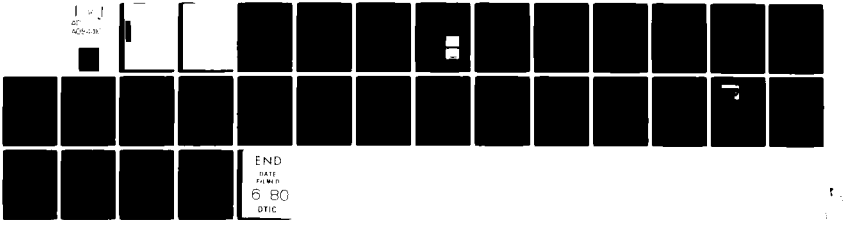

InP: Fe-DOPED
PSG ENCAPSULATION
750 °C, 15-min. ANNEALS
18-DD-15445-2
1 x 10^14 cm^-2
400-keV Se+ (n-type)
1 x 10^14 cm^-2
400-keV Cd (p-type)

(12)

MASSACHUSETTS INSTITUTE OF TECHNOLOGY

LINCOLN LABORATORY

ELECTROOPTICAL DEVICES

SEMIANNUAL TECHNICAL SUMMARY REPORT
TO THE
ROME AIR DEVELOPMENT CENTER

1 APRIL – 30 SEPTEMBER 1979

ISSUED 24 MARCH 1980

LEXINGTON MASSACHUSETTS

ABSTRACT

This report covers work carried out with support of the Department of the Air Force during the period 1 April through 30 September 1979. A part of this support was provided by the Rome Air Development Center.

The current objectives of the electrooptical device program are: (1) to perform life tests on GaInAsP/InP double-heterostructure (DH) diode lasers operating in the 1.0- to 1.3-μm wavelength region and analyze the degradation mechanisms, and (2) to fabricate and study avalanche photodiodes of similar composition GaInAsP operating in the same wavelength region.

Self-sustained pulsations in light output, similar to those occurring in AlGaAs lasers, ~~have been~~ were studied in GaInAsP DH lasers. In marked contrast to observations for AlGaAs lasers, the rate of incidence of the pulsations is much lower and their occurrence does not appear to be increased by aging. The pulsations appear to be related to defects originating in the growth process or subsequent fabrication procedures.

Substantial increase in avalanche gain and reduction of dark current have been achieved in a modified version of the inverted-mesa GaInAsP/InP avalanche photodiode structure. Dark currents as low as 1.5 nA at half the breakdown voltage and photocurrent gains as high as 700 have been measured.

Implantation of the donors Se, Si, and C and the acceptors Cd, Mg, and Be from room temperature to 200°C ~~has been~~ were studied. The sample temperature during implantation is found to have a pronounced effect on the electrical characteristics of the resulting layers. Electron concentrations in excess of 10^{19} cm^{-3} have been achieved.

A vector formulation has been devised to describe quantitatively the change in lattice parameters as a function of composition of the alloy $Ga_xIn_{1-x}As_yP_{1-y}$. The technique has potential use in the further development of lattice-matched $Ga_xIn_{1-x}As_yP_{1-y}$ heterostructure lasers and photodetectors.

The diffusion of Zn and Cd into InP has been investigated in order to make a comparative evaluation of these elements as acceptor diffusants for the fabrication of GaInAsP/InP electrooptical devices. The use of Zn is found to be advantageous because p-n junctions with comparable characteristics are obtained with lower diffusion temperatures than those required for Cd.

micrometer

10 to the 17 power per cc were achieved.

CONTENTS

	Abstract	iii
I.	SELF-SUSTAINED PULSATIONS IN GaInAsP/InP DH LASERS	1
II.	GaInAsP/InP AVALANCHE PHOTODIODES	7
III.	THE EFFECT OF IMPLANT TEMPERATURE ON THE ELECTRICAL CHARACTERISTICS OF ION-IMPLANTED InP	11
	A. Introduction	11
	B. Experimental Procedures	11
	C. Heavy Ions	11
	D. Light and Intermediate-Mass Ions	17
	E. Summary	18
IV.	CHANGES IN LATTICE PARAMETER AND COMPOSITION OF $Ga_xIn_{1-x}As_yP_{1-y}$: A VECTOR FORMULATION	19
V.	DIFFUSION OF Zn AND Cd IN InP	21
	References	25

ELECTROOPTICAL DEVICES

I. SELF-SUSTAINED PULSATIONS IN GaInAsP/InP DH LASERS

As we reported previously,[1] self-sustained pulsations in the light output of CW, room-temperature GaInAsP double-heterostructure (DH) lasers have been observed. Although this pulsation phenomenon is similar to that reported[2-7] for AlGaAs lasers, we find that the rate of incidence is much lower in the GaInAsP devices. Also, in marked contrast to AlGaAs devices,[3,7] it does not appear that aging increases the occurrence of self-pulsing.

The lasers for this study were fabricated from wafers prepared by liquid-phase epitaxial growth of double heterostructures on InP substrates.[8] Tests were made on 156 unaged devices, 10 devices aged at 22°C, and 6 aged at higher temperature – the aging times ranging from hundreds to many thousands of hours, as will be discussed later. All devices had 13- to 15-μm-wide stripes defined by proton bombardment,[9] except for two aged devices with Schottky-barrier-defined (SBD) stripes[10] 7.5 μm in width. All the lasers operated CW at room temperature with emission wavelengths in the 1.2- to 1.3-μm region. The two longest-lived devices are still operating with accumulated operating times of 11,000 and 12,600 h, with the former showing no increase in threshold.

Figure I-1(a-b), taken from a previous report,[1] shows the light output vs time, measured with a Ge photodiode, for two unaged GaInAsP lasers excited with 70-nsec pulses. Trace (a) is for a device exhibiting the usual damped relation oscillation, while trace (b) is for a device in

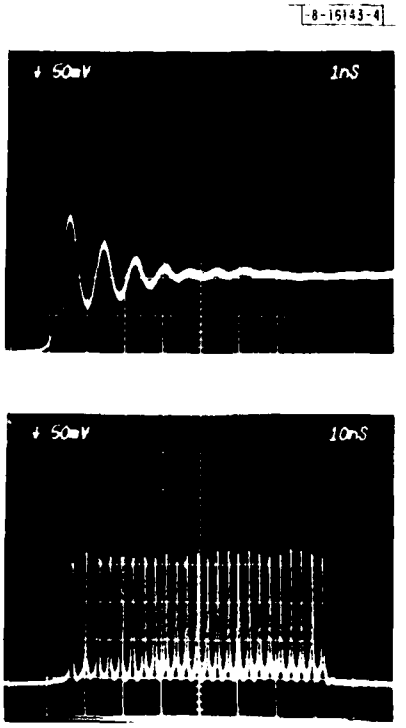

Fig. I-1. Transient response of two GaInAsP lasers for 70-nsec current pulses showing (a) damped relaxation oscillations (1 nsec per div.) and (b) undamped pulsations (10 nsec per div.). Apparent pulsation width is instrument-limited here but is ~100 psec when measured with a high-speed detector and sampling oscilloscope.

TABLE I-1

AGING CONDITIONS FOR LASERS TESTED FOR PULSATIONS

Time (h)	Equivalent* Time at 22°C (h)	Temperature (°C)	Operating Current Density (kA/cm^2)	Comments (see text)
12,600†	–	22	11.5	7.5-μm SBD
11,100‡	–	22	3.2	Wafer 4-4-78
11,000	–	22	7.1	7.5-μm SBD
7,800	–	22	5.5	–
5,800	–	22	8.1	–
3,400†	–	22	7.8	–
3,400†	–	22	6.4	–
3,000	–	22	7.0	–
2,400	–	22	6.9	Weak pulsations
2,100	–	22	12.3	–
882	4,400	40	9.1	–
1,200	13,000	50	4.2	Wafer 4-4-78
1,000‡	11,000	50	4.0	Wafer 4-4-78
212	2,300	50	8.1	–
184	2,000	50	8.0	–
482	–	90	0	Wafer 4-4-78

*Assuming $E_a = 0.7$ eV.

† Still operating

‡ Still operating with no change in threshold.

which the output consists of undamped pulsations. With DC excitation, these pulsations continue indefinitely. The width (measured with a high-speed GaInAsP detector[11] and a sampling oscilloscope to be $\lesssim$100 psec in the device shown) and amplitude of the pulsations do not vary significantly with current amplitude, but the repetition rate increases from approximately 100 MHz near threshold up to approximately 1 GHz well above threshold. The pulsations are suppressed for currents near the nonlinear "kinks" in the light output vs current characteristics, as reported[5] for AlGaAs devices.

Of our 156 unaged devices, which were fabricated from 8 different wafers, only 8 exhibited self-sustained pulsations, for an average rate of incidence of 5 percent. Six of these came from a single wafer (wafer 4-4-78, whose performance characteristics have been described earlier[12]) that provided 58 of the devices tested. For the other 7 wafers, only 2 out of 98 devices exhibited pulsations. For comparison, in a study of proton-bombarded AlGaAs lasers, Paoli[3] reported initial rates of incidence ranging from 5 to 30 percent for 4 wafers, with an average rate of 20 percent. More recently, Hartman et al.[7] have reported an initial rate of incidence of pulsations of 38 percent for 47 strip-buried-heterostructure AlGaAs lasers.

Experiments on AlGaAs lasers have shown that the occurrence of sustained pulsations is strongly increased by aging. Thus, Paoli[3] found that an average of 62 percent (48 to 70 percent, depending on the wafer) of 103 initially nonpulsing devices had developed some degree of sustained pulsations after CW operation at 70°C for 50 to 60 h (equivalent to operation at 22°C for 2,300 to 4,800 h, if the activation energy is assumed to be 0.7 to 0.8 eV). Moreover, Hartman et al.[7] found that 5 out of 10 lasers which did not initially exhibit pulsations did so after only 15 h of CW operation at 35°C (equivalent to 55 h at 22°C). To investigate the effect of aging on self-sustaining pulsations in GaInAsP lasers, we tested 16 devices that had been subjected to the aging conditions summarized in Table I-1. All but one had been operated CW for more than 2,000 h at 22°C (or an equivalent time at higher temperature, assuming an activation energy of 0.7 eV) with approximately 3 mW of output power per facet. The other device had been baked at 90°C without current flow until degradation was evident after 482 h. Four devices were from wafer 4-4-78, which had the highest initial incidence of lasers with sustained pulsations. All devices were aged in air without facet coatings and, except for the devices from wafer 4-4-78, operating current densities were quite high.

After aging, only one device (from wafer 8-18-77, operated at 22°C for 2,400 h) showed pulsations, and these were weak compared with those illustrated in Fig. I-1(b). Even in this case it is not certain that the pulsations were induced by aging, since initial screening for sustained pulsations was not done at the time the device was put on test. For the device still operating unchanged at 50°C, we found no change in the relaxation oscillation transient at 22°C for the same pulsed current when we compared photographs taken before and after aging. Although such a comparison could not be made for the other devices, since photographs were not taken before aging, we found no cases of unusually low damping of the oscillations after aging, which might indicate the initial stages of a shift toward undamped pulsations. Overall, the results of the aging experiments strongly suggest that sustained pulsations will not occur to a significant degree in the first 10,000 h or so of room-temperature operation of initially nonpulsing GaInAsP lasers.

In Fig. I-2 we have plotted threshold current density vs reciprocal device length for all 58 unaged devices from wafer 4-4-78. For ideal devices with no localized optical or electrical defects, the dependence of threshold on reciprocal length should be essentially linear with a

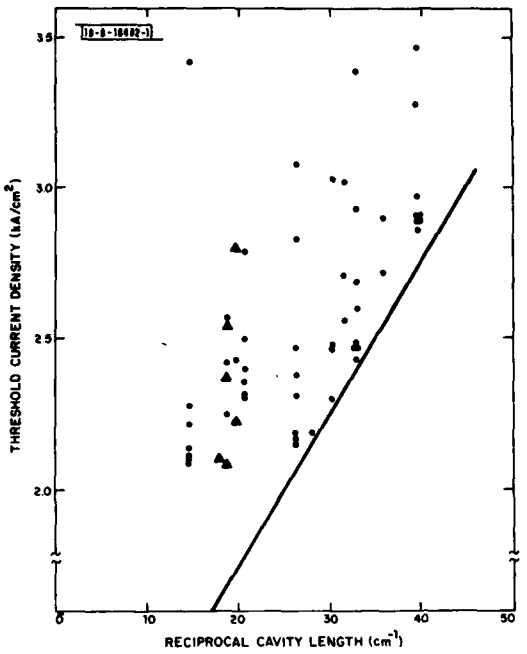

Fig. I-2. Threshold current density vs reciprocal cavity length for 58 unaged lasers from wafer 4-4-78. Triangular data points correspond to devices exhibiting sustained pulsations. Solid line represents dependence suggested by overall trend of data which would exist for defect-free devices.

positive slope. In the presence of random localized defects, the observed thresholds should be scattered and lie above the ideal, minimum values. This is apparently the case for the data of Fig. I-2, where the solid line has been drawn to represent the ideal, defect-free relationship suggested by the overall trend of the data. The circled data points represent the 6 devices with sustained pulsations. Since all 6 are approximately 545 μm long, it is likely that they are all from the same cleaved bar. (The wafer is first cleaved into bars before individual devices are cut.) Since several devices of comparable length to these 6 devices, as well as several slightly shorter and several somewhat longer, do not exhibit sustained pulsations, length does not appear to be an important factor. Moreover, since the threshold current densities of the devices with sustained pulsations vary from the lowest observed in this wafer to among the highest, defects contributing to increased threshold are not necessarily related to the phenomenon. Instead, it appears that defects peculiar to one particular cleaved bar, and hence to one region of the wafer, are responsible for the sustained pulsations in this case. Such localized defects could result from irregularities in the growth process or fabrication procedures.

In their work with AlGaAs lasers, Hartman et al.[7] demonstrated that the occurrence of pulsations was correlated with the presence of absorbing defects classified as either grown-in crystalline defects, dark-line defects, or darkening adjacent to the mirrors, the latter two defects being associated with degradation due to aging. Early observations[13] of long operating life in GaInAsP lasers suggested that these devices might not be subject to the same degradation mechanisms that occur in AlGaAs lasers. More recent studies[14] have shown that relatively few dark-line defects are observed in GaInAsP lasers even after extensive aging, and that much of the degradation which is observed in these devices may be due to problems associated with the use of indium solder,[15,16] as we have previously observed.[1,12] Darkening adjacent to mirrors is thought to be due to rapid nonradiative recombination at the cleaved surface.[17] There is

evidence[18] that surface recombination velocity in n-InP is much lower than in n-GaAs. If this should prove true of GaInAsP alloys, darkening adjacent to the mirrors might also prove to be less of a problem even when devices are operated in air without facet coatings, as in the present case.

Further studies of self-sustained pulsations in these lasers are under way, including measurements of gain vs current in devices both with and without pulsations.

J. N. Walpole J. J. Hsieh
T. A. Lind A. G. Foyt

II. GaInAsP/InP AVALANCHE PHOTODIODES

Substantial increase in avalanche gain and reduction of dark current have been achieved in a modified version of the inverted-mesa GaInAsP/InP avalanche photodiode structure described previously.[19,20] The structure, shown in Fig. II-1, differs from the earlier one in that a 1-μm layer of n-InP is interposed between the p^+-InP substrate and the n-GaInAsP layer. (The n^+-InP top layer is also omitted for simplicity, with little expected effect other than some increase in contact resistance and a possible decrease in quantum efficiency due to surface recombination of photogenerated carriers.) The p-n junction is now located in the InP, but with sufficient reverse bias the depletion region extends into the GaInAsP. Hence, incident light of appropriate wavelength ($\lambda \lesssim 1.3$ μm) is absorbed in the GaInAsP, generating holes which are swept into the InP where they are multiplied in the high-field region of the junction. This separation of the generation and multiplication regions and the attendant improvement in avalanche detector characteristics of GaInAsP/InP photodiodes were first demonstrated by Nishida et al.[21,22] in a diffused structure. In the devices described here, the diffusion step is not required and edge breakdown is clearly eliminated by use of the inverted-mesa structure.[19,20]

Details of the structure used in these initial studies are given in Fig. II-1. Layers of n-type InP and GaInAsP with $n \approx 1 \times 10^{16}$ cm^{-3} are grown onto a p^+-InP substrate by liquid phase epitaxy. The InP and GaInAsP layers have thicknesses of 1 and 3 μm, respectively. The approximate composition of the quaternary alloy was $Ga_{0.23}In_{0.77}As_{0.52}P_{0.48}$ with the long-wavelength photoresponse cutoff measured to be about 1.25 μm. Mesas, 8 μm in height, were etched using a mask that yields devices of 6 different diameters, ranging from 2.5 mils (64 μm) to 6 mils (152 μm). Plated AuSn top contacts, 1 mil in diameter, and an evaporated AuMg bottom contact were alloyed by heating the sample to ~400°C for 10 sec. The AuMg contact did not cover the entire back surface, thus leaving windows through which to shine light from the back side. A layer of Si_3N_4, approximately 900 Å thick, was used as surface passivation and antireflection coating.

Best results were obtained on the smaller devices (2.5 to 3.5 mils in diameter). I-V characteristics, a typical one of which is shown in Fig. II-2, gave dark currents as low as 1.5 nA at $1/2\ V_B$. (V_B, the breakdown voltage, was approximately 100 V in these devices.) Scanning the devices with 1.15-μm laser light, incident from both the front and back sides, yielded uniform photoresponse. Taking into account approximately the variation in collection efficiency with bias, maximum low-frequency gains of up to ~700 were observed with ~2 nA of primary photocurrent induced by light incident on the back sides; lower gains (~200) were measured when light of the same intensity was incident from the front. The reason for the difference in gain as measured from the front and back is not presently understood. In both cases, the light is predominantly absorbed in the n-GaInAsP layer and, hence, the carriers initiating the multiplication are primarily holes. Although changes in collection efficiency with bias are much more pronounced with light incident from the front, our initial calculations indicate that any reasonable estimate of this variation does not account for the apparent gain difference. The maximum gain from both front and back was observed to decrease with increasing primary photocurrent over the range from 2 nA to 1 μA (at which the maximum gain measured was ~10, from both front and back).

No photoresponse was observed at biases below 12 V. At this value of bias, a current step was observed in the I-V characteristics of the devices under illumination with a microscope lamp

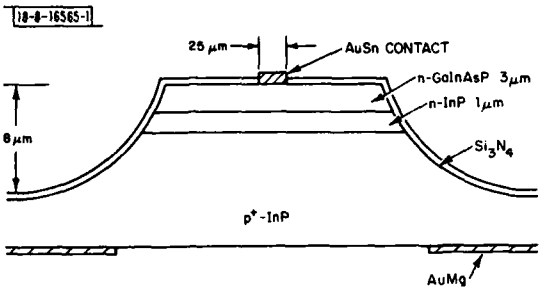

Fig. II-1. Schematic cross section of GaInAsP/InP inverted-mesa avalanche photodiode with p-n junction located in InP. Device diameters range from 2.5 to 6 mils.

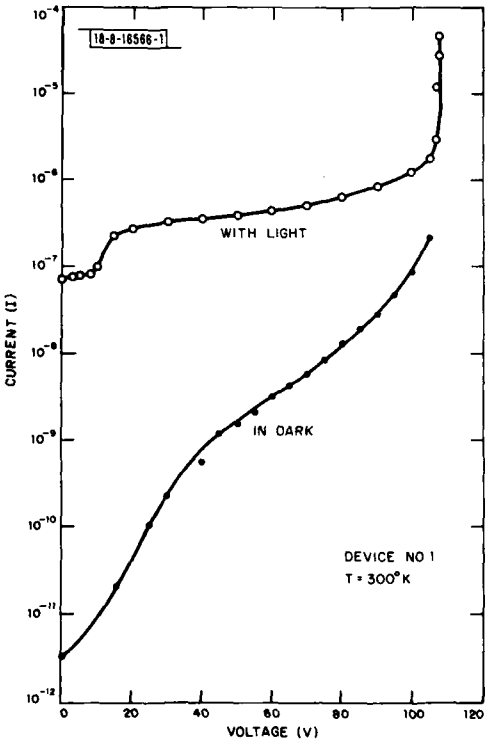

Fig. II-2. I-V characteristics of structure shown in Fig. II-1. Closed circles correspond to dark current; open circles were taken with device illuminated by a microscope lamp.

(see Fig. II-2), and a discontinuity occurred in the concentration profile obtained from C-V measurements. These discontinuities are expected at the value of applied bias for which the depletion region punches through the InP/GaInAsP heterojunction. The photogenerated holes, which at low bias had been confined to the GaInAsP by the valence-band barrier of the heterojunction, are now swept by the junction field over the barrier into the InP where they are collected.[21,22]

With the 1.06-μm, 200-psec-pulse excitation from a mode-locked Nd:YAG laser incident from the front of a typical device, response times of ~400 psec (FWHM) were measured. This relatively long response time is probably due to the fact that, with light incident from the front, carriers generated at the surface must diffuse through a large portion of the quaternary layer before reaching the field region. No such diffusion takes place with light incident from the back, hence shorter response times are expected.

Work is presently under way to further characterize the devices with respect to spectral response, noise characteristics, and frequency response, as well as to optimize device parameters.

V. Diadiuk
S. H. Groves
C. E. Hurwitz

III. THE EFFECT OF IMPLANT TEMPERATURE ON THE ELECTRICAL CHARACTERISTICS OF ION-IMPLANTED InP

A. INTRODUCTION

The expanding interest in InP devices during the last few years has led, in turn, to increased activity in the development of ion-implantation technology in this material.[23-34] Many of the results previously published[23,24,28,33] have indicated that the temperature of the InP during implantation can have a pronounced influence on the characteristics of the resulting implanted layers. In this section, new and more detailed results are presented of a study of these temperature effects on the electrical characteristics of InP layers implanted with several donor (C, Si, and Se), acceptor (Be, Mg, and Cd), and nondoping (Kr) impurities.

B. EXPERIMENTAL PROCEDURES

The InP samples used in these experiments were cut from (111)-oriented high-resistivity ($\rho \geq 10^7$ Ω-cm) Fe-doped crystals. The samples were lapped, polished, and etched[35] in a 1:1:5:1 mixture of HAc:$HClO_4$:HNO_3:HCl. During implantation, they were tilted in reference to the ion beam to minimize channeling. Following implantation, the samples were annealed at 750°C for 10 to 15 min. using a PSG (phosphosilicate glass) encapsulation technique described previously.[23,28] Microalloyed Au-Sn was used to contact implanted n-type layers, while microalloyed Au-Zn or Au-Mg was used for p-type layers. Cloverleaf patterns etched in the implanted layers facilitated Hall measurements of the van der Pauw type.[36] Unimplanted control samples of the Fe-doped InP used in these experiments, which were similarly temperature-cycled in the ion-implantation system, encapsulated and annealed at temperatures up to 800°C, showed no indication of the formation of surface conducting layers.

C. HEAVY IONS

Previous results indicated that higher sheet carrier concentrations are obtained by implanting heavy ions into InP at 200°C rather than at room temperature.[23] Figure III-1 shows the sheet carrier concentration vs implant temperature of InP samples implanted with 1×10^{14} cm^{-2} of a heavy n-type impurity (Se), a heavy p-type impurity (Cd), and a heavy inert species (Kr). All the ions were implanted at an energy of 400 keV.

1. Krypton (Damage Effects)

The Kr implants were performed in an attempt to determine the electrical behavior of residual damage in InP implanted with heavy ions. Assuming that the Kr itself is not electrically active, the data in Fig. III-1 show that residual ion-implantation damage in InP is n-type.[23,37] For room-temperature Kr implants, the sheet carrier concentration consistently falls in the range of (5 to 6) $\times 10^{12}$ cm^{-2} with corresponding sheet mobilities of several hundred cm^2/V-sec. This measured sheet carrier concentration, which is presumably due to the effects of residual damage, decreases with increasing implant temperature. For samples implanted at temperatures of 100°C and above, the concentration is much lower than for those implanted at room temperature, ranging from not measurable ($<10^9$ cm^{-2}) to about 2×10^{11} cm^{-2}. There is, however, considerable scatter in the data for 100° to 200°C implant temperatures and only data points indicating the range of measured sheet concentration have been included in Fig. III-1. The

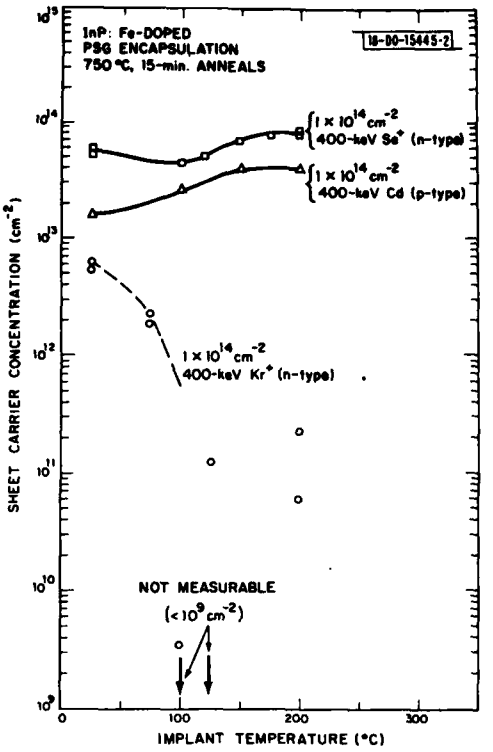

Fig. III-1. Sheet carrier concentration vs implant temperature for InP samples implanted with 1×10^{14} cm^{-2} of heavy ions, 400-keV Se (an n-type impurity), Cd (a p-type impurity), and Kr (a neutral species).

ambiguity of the results above 100°C indicates that other mechanisms which contribute to the observed sheet carrier concentrations are becoming significant. One possibility is that damage-enhanced outdiffusion of P and/or compensating impurities or defects is occurring during the heated implant. Nevertheless, the data clearly indicate that implant temperatures $\geq$100°C are necessary to minimize the n-type behavior due to the residual damage induced by the implantation of heavy ions in InP. It should be further noted that, even for heated implants, the post-implantation anneal is essential. For example, unannealed samples implanted at 200°C with 1×10^{14} cm^{-2} of Kr had sheet concentrations in the range of $(2 \text{ to } 3) \times 10^{12}$ cm^{-2} and very low sheet mobilities [(5 to 10) cm^2/V-sec]. Similar samples annealed at 750°C for 15 min. had sheet concentrations of $(6 \text{ to } 20) \times 10^{10}$ cm^{-2} and much higher mobilities [(420 to 1100) cm^2/V-sec].

2. Selenium

As shown in Fig. III-1, samples implanted with the donor ion Se at temperatures above 150°C had higher sheet carrier concentrations than those implanted at room temperature. The sheet mobilities for the heated implants [(1700 to 1800) cm^2/V-sec] are also higher than for those done at room temperature [(1150 to 1450) cm^2/V-sec]. The small decrease in the measured sheet carrier concentration for samples implanted between room temperature and 100°C is believed to be due to a decrease in the number of donor levels resulting from the above-mentioned residual n-type implant damage. Above 100°C, the sheet carrier concentration increases with implant temperature until it saturates at $(7.8 \text{ to } 8.0) \times 10^{13}$ cm^{-2}. For ten samples implanted at 200°C, all had sheet carrier concentrations in the range $(7.8 \text{ to } 8.0) \times 10^{13}$ cm^{-2} and all

but one (which had a sheet mobility of 1900 cm^2/V-sec) had sheet mobilities in the range (1700 to 1800) cm^2/V-sec.

To examine the effects of implant temperature on the depth profile of the electrically active implanted Se, a series of Hall measurements combined with step etching[38] was performed on selected samples. Figure III-2 shows the carrier concentrations and mobilities vs depth of two InP samples, one implanted at 200°C and one at room temperature, both with 1×10^{14} cm^{-2} of 400-keV Se. Also shown is the theoretical Se profile calculated using the Johnson and Gibbons formulation[39] of LSS theory.[40] The sample implanted at 200°C has a peak concentration of about 3.8×10^{18} cm^{-3} at a depth of 1650 Å, in agreement with the theoretical range of LSS theory. The distribution of the carrier concentration, however, is wider than expected from LSS theory, indicating that some diffusion of the Se is taking place during the implant and/or the anneal. For the sample implanted at room temperature, the Se near the surface is either not electrically active or compensated. The mobility of the sample implanted at room temperature is lower than that of the sample implanted at 200°C at all depths.

Samples implanted with doses of 400-keV Se from 1×10^{13} to 1×10^{15} cm^{-2} showed similar behavior of the sheet carrier concentration vs implant temperature, as did the samples implanted with 1×10^{14} cm^{-2}. Figure III-3 shows the carrier concentration vs depth for samples implanted at 200°C with 3×10^{13}, 1×10^{14}, and 1×10^{15} cm^{-2} 400-keV Se. All the samples had the peak of the carrier concentration at the depth expected from LSS theory, but the distributions were again wider than predicted. The sample implanted with a Se dose of 1×10^{15} cm^{-2} had a peak carrier concentration of 1.6×10^{19} cm^{-3}, indicating that electron concentrations in excess of 10^{19} cm^{-3} can be fairly easily achieved in InP with implanted Se.

3. Cadmium

For the heavy p-type impurity (Cd), Fig. III-1 shows that the sheet carrier concentration increases with implant temperature and that implant temperatures of 150°C or above are required for highest activation. However, the sheet hole concentrations, even for implant temperatures above 150°C, are only 4.0×10^{13} cm^{-2}, corresponding to an effective activation of 40 percent – a value which is low compared with the 78- to 80-percent activation achievable with the n-type impurity Se.

Figure III-4 shows the sheet hole concentration and mobility vs dose for samples implanted with 400-keV Cd at room and several higher temperatures. The sheet mobility does not appear to be very dependent on implant temperature. The highest sheet concentration obtained, measured on a sample implanted with 1×10^{15} cm^{-2} at 150°C, was 9×10^{13} cm^{-2}, with a corresponding sheet mobility of 100 cm^2/V-sec.

As has been observed in GaAs (see Refs. 41 and 42), there appears to be substantial diffusion of the implanted Cd. This is illustrated in Fig. III-5, where the hole carrier concentration and mobility vs depth are plotted for a sample implanted at 200°C with 1×10^{14} cm^{-2} of 400-keV Cd. Also shown is the implanted Cd profile expected from LSS range theory. The measured peak hole concentration is only 1.5×10^{18} cm^{-3}, and the profile is much wider than expected. Although additional experiments are required to more fully determine the effects of dose and implant temperature on diffusion, it appears that it will be more difficult to obtain high hole concentrations in InP by ion implantation than it is in GaAs (see Refs. 41 and 42).

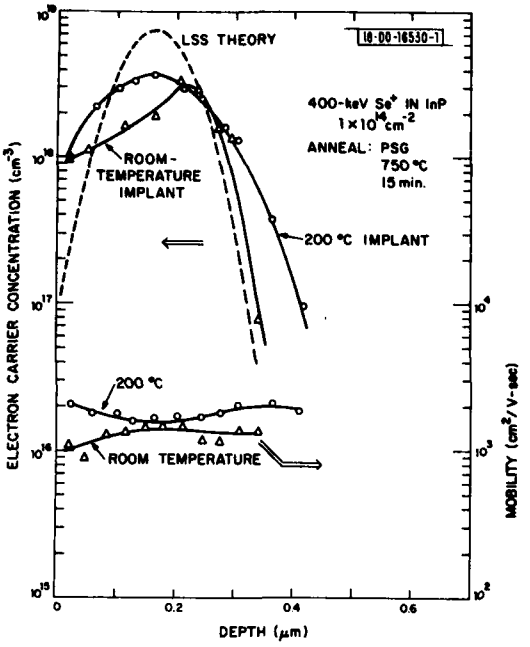

Fig. III-2. Electron carrier concentration and mobility vs depth measured in InP implanted at room temperature and 200°C with 1×10^{14} cm^{-2} of 400-keV Se ions. Also shown is Se distribution expected from LSS range theory.

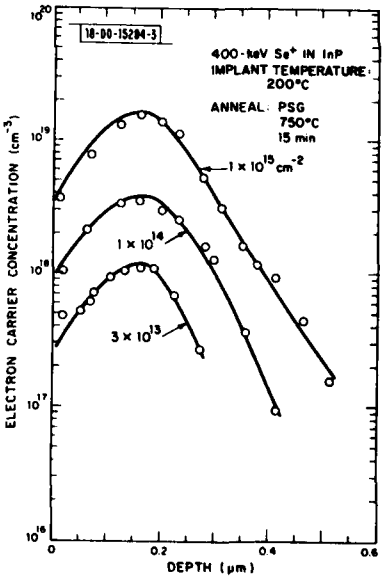

Fig. III-3. Electron carrier concentration vs depth for InP samples implanted at 200°C with 3×10^{13}, 1×10^{14}, and 1×10^{15} cm^{-2} of 400-keV Se.

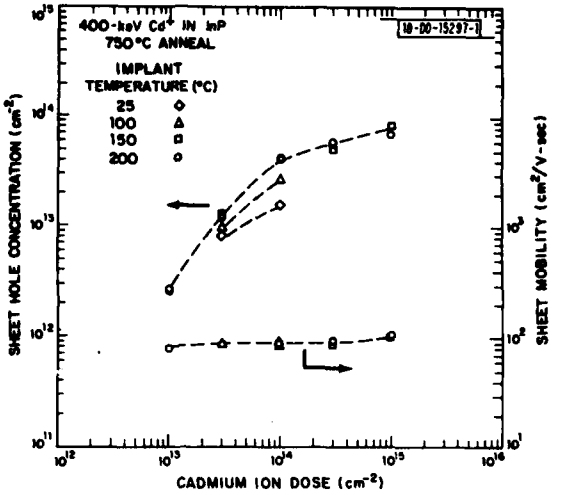

Fig. III-4. Sheet hole concentration and mobility vs dose for InP samples implanted at room temperature, 100°C, 150°C, and 200°C with 400-keV Cd ions.

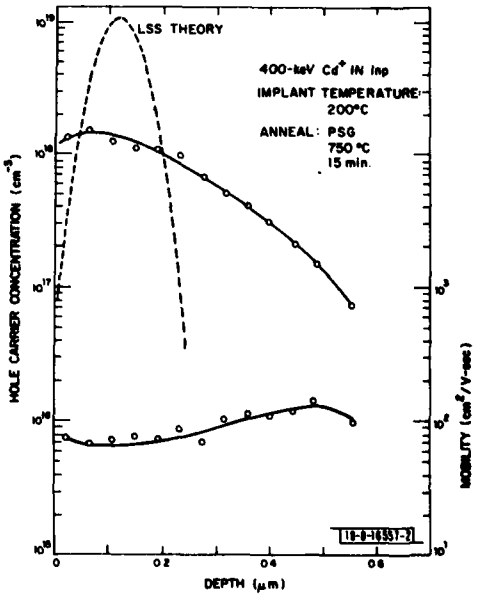

Fig. III-5. Hole carrier concentration and mobility vs depth for an InP sample implanted at 200°C with 1×10^{14} cm^{-2} of 400-keV Cd.

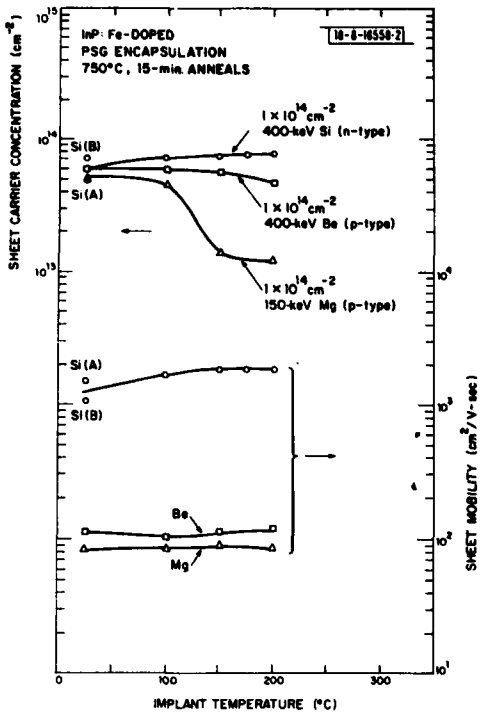

Fig. III-6. Sheet carrier concentration and mobility vs implant temperature for InP samples implanted with 1×10^{14} cm^{-2} of 400-keV Be (a light ion), and 1×10^{14} cm^{-2} of 400-keV Si and 150-keV Mg (ions of intermediate mass). Points A and B for Si data represent highest and lowest measured sheet carrier concentrations.

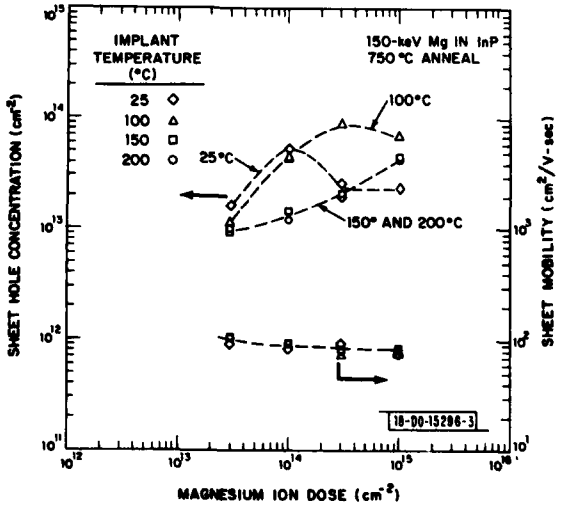

Fig. III-7. Sheet hole concentration and mobility vs dose for InP samples implanted at room temperature, 100°C, 150°C, and 200°C with 150-keV Mg ions.

D. LIGHT AND INTERMEDIATE-MASS IONS

Results obtained on the implantation of lighter ions are shown in Fig. III-6, where the sheet carrier concentration and mobility of samples implanted with 1×10^{14} cm^{-2} of a light ion (400-keV Be) and two ions of intermediate mass (400-keV Si and 150-keV Mg) are plotted as a function of implant temperature. For these lighter ions, n-type conduction due to residual implant damage does not appear to be the problem it is with heavy ions. In confirmation of this conclusion, samples implanted at room temperature with 1×10^{14} cm^{-2} of 400-keV Ne and annealed at 750°C showed no indication of the formation of surface conducting layers. It is also clear from the data that the effects of implant temperature for these lighter ions are much less consistent than for the heavy ions.

1. Beryllium

The sheet hole concentrations obtained for samples implanted with Be at room temperature are slightly higher than those obtained on samples implanted at 200°C. More detailed data on Be-implanted InP (Ref. 28) show that the results of room-temperature Be implants are generally as good as, and in some cases superior to, those of heated implants because of less in-diffusion of the implanted Be. The maximum activation obtained for this light p-type impurity, approximately 60 percent, is again less than that obtained with n-type impurities.

2. Carbon

The implantation of carbon, another possible light impurity in InP, was found to result in n-type layers, but with only 4- to 6-percent apparent electrical activity, independent of implant temperature. The results indicate that implanted carbon is probably highly amphoteric, although the possibility that the carbon occupies interstitial sites is not ruled out. This contrasts with results reported for GaAs (see Ref. 43) in which implanted carbon was found to be p-type with up to 50-percent effective doping efficiency.

3. Silicon

For the intermediate-mass n-type impurity (Si), higher sheet carrier concentrations and mobilities were generally obtained on samples implanted at elevated temperatures. As indicated in Fig. III-6, there is considerable scatter in the room-temperature results, while for samples implanted at 200°C with 1×10^{14} cm^{-2} of 400-keV Si, the measured sheet carrier concentrations and mobilities all fell in the ranges $(7.6 \text{ to } 7.8) \times 10^{13}$ cm^{-2} and (1800 to 2000) $cm^2/V\text{-sec}$, respectively.

4. Magnesium

For samples implanted with Mg at 150 keV and a dose of 1×10^{14} cm^{-2}, higher sheet hole concentrations were obtained on those implanted at room temperature than on those done at higher temperatures. In contrast to the other ions studied, however, the results obtained with Mg implanted at room temperature exhibit an anomalous dependence on dose. This can be seen in Fig. III-7, where the sheet hole concentration and mobility of InP samples implanted with 150-keV Mg at several temperatures are plotted vs dose. For the room-temperature implants, the sheet hole concentration increases with implant dose up to 1×10^{14} cm^{-2}, whereas for doses above this value the sheet hole concentration actually falls quite drastically. For 100°C implants,

a less-abrupt maximum is observed at a dose of 3×10^{14} cm^{-2}, while for implants performed with the InP at temperatures of 150°C or above, the sheet hole concentration increases monotonically with dose. Profile measurements on samples implanted at room temperature with 1×10^{14} cm^{-2} Mg indicate that significant diffusion of the implanted Mg occurs. Although more work is needed to fully understand the data in Fig. III-7, a plausible explanation may be based on a combination of: (a) a damage-enhanced diffusion effect which decreases with increasing implant temperature, and (b) a critical dose, above which significant residual n-type damage remains after annealing, and the value of which increases with implant temperature. This critical dose, which could be that at which amorphization occurs, becomes extremely high and, for all practical purposes, infinite[44] for implant temperatures of 150°C and above. Referring to Fig. III-7, the sheet mobility does not seem to depend critically on implant temperature. The highest sheet hole concentration obtained by implanting 150-keV Mg was 9×10^{13} cm^{-2} with a corresponding sheet mobility of 80 $cm^2/V\text{-sec}$. These results were obtained on a sample implanted at 100°C with a dose of 3×10^{14} cm^{-2}.

E. SUMMARY

The results indicate that to achieve the highest activation of both heavy n-type impurities (e.g., Se) and heavy p-type impurities (e.g., Cd), ion implantation in InP should be carried out with the InP at temperatures of 150°C or above. It is interesting to note that an implant temperature of 150°C corresponds to that above which InP cannot be made amorphous by ion implantation.[44] For the light-ion Be, room-temperature implants are generally as good as, and in many cases superior to, heated implants. The intermediate-mass n-type impurity (Si) behaves more like the heavy ions, and implants carried out with the InP substrates at temperatures of 150°C or above generally result in higher carrier concentrations and mobilities. For the intermediate-mass p-type dopant (Mg), the effects of implant temperature appear to be dependent on dose. This behavior is not well understood and it is likely that the particular application may determine the most-effective implant parameters for Mg.

It is also evident from the data that implanted n-type dopants, such as Se and Si, have higher electrical activities in InP than p-type dopants, and that electron carrier concentrations $>10^{19}$ cm^{-3} are relatively easy to achieve. This is in contrast to results obtained on GaAs, in which it is generally easier to obtain higher activation efficiencies and peak concentrations with p-type impurities.[45]

J. P. Donnelly
C. E. Hurwitz
G. A. Ferrante

IV. CHANGES IN LATTICE PARAMETER AND COMPOSITION OF $Ga_xIn_{1-x}As_yP_{1-y}$: A VECTOR FORMULATION

There have been extensive studies on the relation between the $Ga_xIn_{1-x}As_yP_{1-y}$ lattice parameter and its composition.[46-48] We have developed a vector formulation in which the change of $Ga_xIn_{1-x}As_yP_{1-y}$ lattice parameter is related to the change in composition in a simpler and clearer way. We believe that this technique is potentially useful in the development of lattice-matched $Ga_xIn_{1-x}As_yP_{1-y}$/InP double-heterostructure lasers.

In this new formulation, change of the lattice parameter is expressed as the scalar product of a vector $\vec{A}$ and the "composition displacement vector" $\vec{\Delta} \equiv \vec{e}_x\Delta x + \vec{e}_y\Delta y$, where $\vec{e}_x$ and $\vec{e}_y$ are unit vectors in the x- and y-directions, respectively. Based on Vegard's law, the vector $\vec{A}$ is constant to within better than 3-percent accuracy over a wide composition range of interest.

It has been reported that the experimentally measured lattice parameter a, as a function of x and y, is in good agreement with Vegard's law,[46,48] i.e.,

$$a = a_{InP}(1-x)(1-y) + a_{InAs}(1-x)y + a_{GaAs}xy + a_{GaP}x(1-y) \qquad \text{(IV-1a)}$$

or

$$a(\mathring{A}) = 5.8696 - 0.4184x + 0.1894y + 0.0130xy \qquad \text{(IV-1b)}$$

by substituting values of a_{InP}, a_{InAs}, a_{GaAs}, and a_{GaP} into Eq.(IV-1a). For small changes in x and y, the corresponding change in a can be obtained by taking the differential of Eq.(IV-1b) which, after some rearranging, becomes

$$\Delta a(\mathring{A}) = (-0.4184 + 0.0130y)\Delta x + (0.1894 + 0.0130x)\Delta y \quad . \qquad \text{(IV-2)}$$

This equation can be written as

$$\frac{\Delta a}{a} = \vec{A} \cdot \vec{\Delta} \qquad \text{(IV-3)}$$

where

$$\vec{A} = \vec{e}_x \frac{-0.4184 + 0.0130y}{5.8696} + \vec{e}_y \frac{0.1894 + 0.0130x}{5.8696} \quad . \qquad \text{(IV-4)}$$

[Since lattice matching to InP is of primary interest, $a \equiv a_{InP} = 5.8696$ Å has been used in Eq.(IV-4).] The vector $\vec{A}$, which is a function of x and y, can be approximated by a constant vector $\vec{A}_o$ which is defined as

$$\vec{A}_o \equiv \vec{e}_x \frac{0.4184}{5.8696} + \vec{e}_y \frac{0.1894}{5.8696} \quad . \qquad \text{(IV-5)}$$

Since the x- and y-values of general interest are $0 \leqslant x \leqslant 0.5$ and $0 \leqslant y \leqslant 1.0$, respectively, the deviations of $\vec{A}$ from $\vec{A}_o$ are smaller than ~3 percent by comparing Eqs.(IV-4) and (IV-5). Another way of obtaining Eq.(IV-3) and $\vec{A} \cong \vec{A}_o$ is illustrated in Fig.IV-1, where the change of lattice parameter in the x-direction is almost independent of y, and vice versa.

Table IV-1 shows the comparison of the present formulation with some experimental results. The compositions of the $Ga_xIn_{1-x}As_yP_{1-y}$ layers were obtained by the electron microprobe technique. The lattice mismatch between the layers and the underlying InP substrates, $(\Delta a/a)_{exp}$ in Table IV-1, were obtained by x-ray diffraction. For comparison with the present technique, one of the four samples is chosen as the reference point, from which the changes in composition,

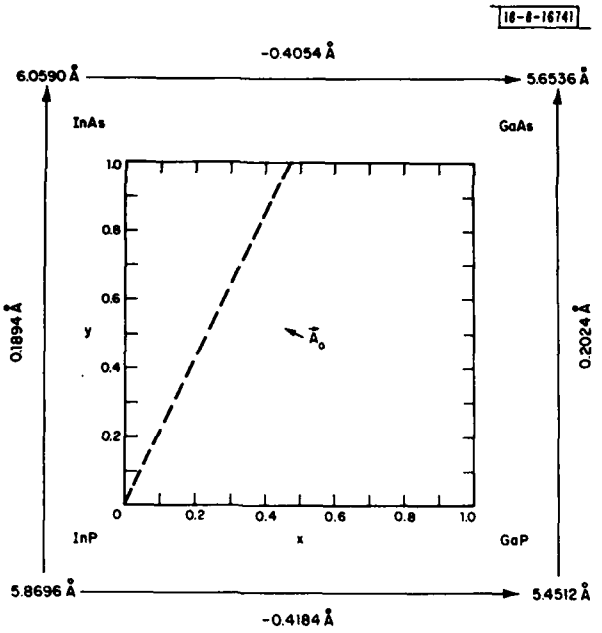

Fig. IV-1. Diagram showing relation between room-temperature lattice parameter and composition in $Ga_xIn_{1-x}As_yP_{1-y}$ system. Dashed curve represents compositions for exact lattice match to InP. Vector $\vec{A}_o$ is that defined in Eq. (IV-5).

TABLE IV-1

COMPARISON OF THE EXPERIMENTAL AND CALCULATED LATTICE-PARAMETER DIFFERENCES OF SOME $Ga_xIn_{1-x}As_yP_{1-y}$ SAMPLES

x	y	$(\Delta a/a)_{exp}$ (percent)	Δx	Δy	$(\Delta a/a)'_{exp}$ (percent)	$(\Delta a/a)_{calculated}$ (percent)
0.2597	0.5914	−0.1	0.0	0.0	0.0	0.0
0.186	0.363	−0.3	−0.0737	−0.2284	−0.2	−0.22
0.177	0.558	0.41	−0.0827	−0.0334	0.51	0.47
0.158	0.667	0.57	−0.1017	0.0756	0.67	0.95

Δx and Δy, and the changes in lattice parameter, $(\Delta a/a)'_{exp}$, were measured. By using Eqs. (IV-3) and (IV-5) and Δx and Δy in Table IV-1, the values of $(\Delta a/a)_{calculated}$ were obtained. There is a good agreement between $(\Delta a/a)_{calculated}$ and $(\Delta a/a)'_{exp}$ except for the largest $\Delta a/a$.

Z. L. Liau
J. J. Hsieh

V. DIFFUSION OF Zn AND Cd IN InP

The elements Zn and Cd are the acceptor impurities commonly used for diffusion from the vapor phase in the fabrication of electrooptical devices employing InP and GaInAsP alloys. High-performance GaInAsP/InP devices such as diode lasers and avalanche photodiodes have been fabricated using Zn and Cd diffusion, respectively. At a given temperature Zn diffuses much faster than Cd, and Zn diffusion can lead to the formation of irregular diffusion fronts. For these reasons, Cd has been suggested as a preferable acceptor diffusant for device fabrication. In order to make a comparative evaluation of the two elements for this purpose, we have carried out a series of experiments on their diffusion in InP. In these experiments, single-crystal n-InP substrates with carrier concentrations of 10^{16} to 10^{18} cm^{-3} were partially masked with SiO_2, Si_3N_4, or phosphosilicate glass (PSG), sealed in evacuated fused-silica ampoules with weighed amounts of ZnP_2 or CdP_2, and heated in a resistance furnace. The depth of the p-n junction formed by diffusion was then determined by cleaving and etching. For Cd diffusion experiments at temperatures above about 550°C, it was necessary to place a small amount of red P in the ampoule to prevent thermal etching of the substrate due to P evaporation. Additional P was not required in the Zn diffusion experiments even at 650°C.

When Zn was diffused at 650°C to form a p-n junction several micrometers deep, the diffusion front was found to be quite flat over most of the sample, but a few defects were observed at the junction. One such defect is seen in Fig. V-1, which is an optical micrograph of a cleaved cross section showing a junction about 4.5 μm deep produced by Zn diffusion at 650°C for 5 min. into a Sn-doped substrate with background carrier concentration of about 10^{18} cm^{-3}. Defects of this type were formed much more often in substrates with such high carrier concentrations than in those with low carrier concentrations ($\sim 10^{16}$ cm^{-3}). No defects were observed for diffusions performed at 500°C or below. The quantitative results of the experiments are shown in Fig. V-2, where the junction depth (L) is plotted against the square root of time ($t^{1/2}$) for Zn diffusions at 500° and 650°C into InP substrates with carrier concentrations of 1 to 2×10^{16}, 3×10^{17}, and 1 to 2×10^{18} cm^{-3}. The data are consistent with a linear dependence of L on $t^{1/2}$. For a given diffusion time and temperature, L is not very sensitive to the substrate carrier concentration.

The diffusion of Cd in InP at 500°C is so slow that no junction was detected even after heating for 40 min. at this temperature. Diffusion at 600°C for about 100 min. yielded a junction depth of about 1 μm, provided that no excess P was added to the ampoule, but in this case the exposed InP surface was severely attacked due to P evaporation. Adding P to prevent thermal etching caused a marked reduction in the rate of diffusion, as reported by Tien and Miller.[49] The diffusion rate reached a limiting value for P/CdP_2 weight ratios of 5 or higher. For such ratios the junction depth was reduced by almost an order of magnitude, so that it would be necessary to employ diffusion temperatures significantly above 600°C in order to obtain useful junction depths in a reasonable time. Severe cracking of passivating coatings occurs at such high temperatures, however, making it impossible to carry out the selective-area diffusion required for device fabrication.

To compare the performance of InP diodes prepared by Zn and Cd diffusion, the dark current under reverse bias has been measured for devices 100 μm in diameter with a p-n junction depth of about 2 μm obtained by diffusion of Zn (20 min. at 500°C) or Cd (100 min. at 600°C, without excess P) into nominally undoped n-InP layers (carrier concentration about 10^{17} cm^{-3}) grown by liquid-phase epitaxy on (100)-oriented substrates. Both types of diodes have the same

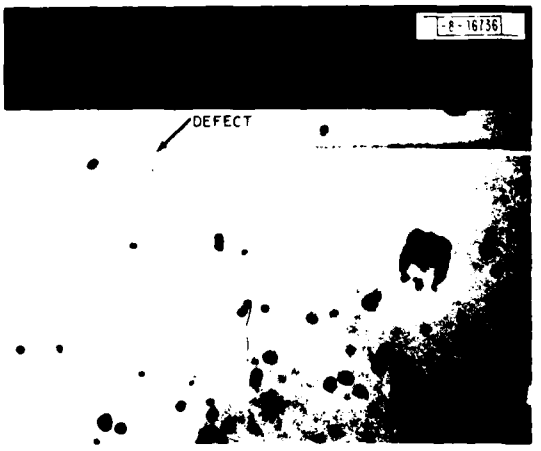

Fig. V-1. Cleaved cross section through an InP sample, showing p-n junction formed at a depth of 4.5 μm by Zn diffusion at 650°C for 5 min. from a ZnP_2 source.

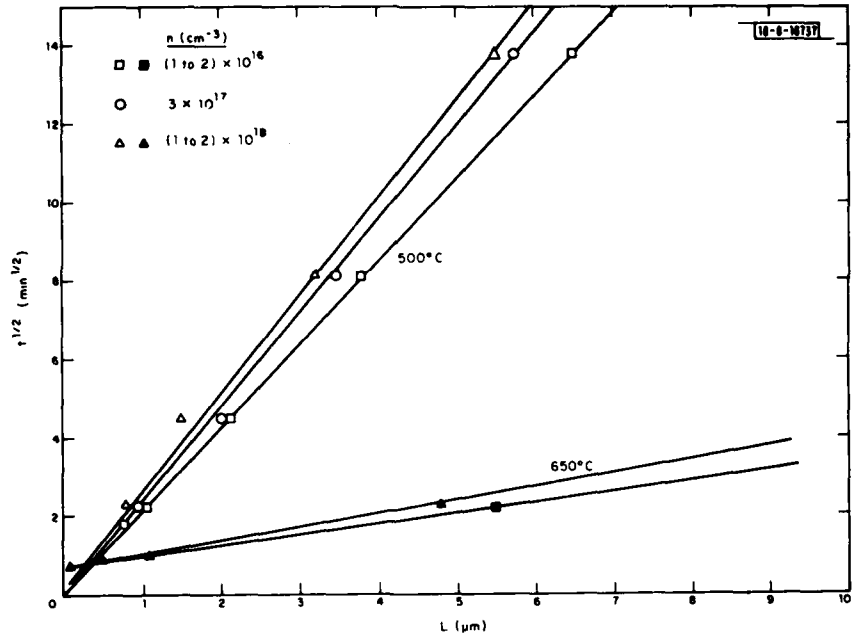

Fig. V-2. P-n junction depth (L) as a function of square root of diffusion time ($t^{1/2}$) for Zn diffusion into n-InP at 500° and 650°C using a ZnP_2 source.

breakdown voltage (V_B = 23 V at 1 μA) and similar leakage currents (2 to 10 nA at 0.5 V_B). The leakage actually depends more strongly on the type of passivating layer than on the acceptor diffusant, with the lowest leakage being obtained for devices from which the passivating layer was removed after diffusion. Since the Zn- and Cd-diffused diodes have comparable characteristics, and Zn diffusion can be readily controlled at temperatures of 500°C or less (making it possible to avoid the difficulties associated with Cd diffusion because of the high temperatures required to obtain practical junction depths), it is advantageous to use Zn rather than Cd as the acceptor diffusant for the fabrication of InP devices.

J. J. Hsieh

REFERENCES

1. Semiannual Technical Summary on Electrooptical Devices, Lincoln Laboratory, M.I.T. (31 March 1979), p. 1, DDC AD-A077152.
2. E. S. Yang, P. G. McMullin, A. W. Smith, J. Blum, and K. K. Shih, Appl. Phys. Lett. 24, 324 (1974).
3. T. L. Paoli, IEEE J. Quantum Electron. QE-13, 351 (1977).
4. G. Arnold and K. Petermann, Opt. Quantum Electron. 10, 311 (1978).
5. J. P. van der Ziel, J. L. Merz, and T. L. Paoli, J. Appl. Phys. 50, 4620 (1979).
6. R. W. Dixon and H. R. Beurier, Appl. Phys. Lett. 34, 560 (1979).
7. R. L. Hartman, R. A. Logan, L. A. Koszi, and W. T. Tsang, J. Appl. Phys. 50, 4616 (1979).
8. J. J. Hsieh, Appl. Phys. Lett. 28, 283 (1976), DDC AD-A025631/3.
9. J. J. Hsieh, J. A. Rossi, and J. P. Donnelly, Appl. Phys. Lett. 28, 709 (1976), DDC AD-A028550/2.
10. J. J. Hsieh, unpublished.
11. Semiannual Technical Summary on Electrooptical Devices, Lincoln Laboratory, M.I.T. (30 September 1978), p. 7, DDC AD-A069091/7.
12. Ibid., p. 2.
13. C. C. Shen, J. J. Hsieh, and T. A. Lind, Appl. Phys. Lett. 30, 353 (1977).
14. T. Yamamoto, K. Sakai, and S. Akiba, IEEE J. Quantum Electron. QE-15, 684 (1979).
15. H. Kressel, M. Ettenberg, and I. Ladany, Appl. Phys. Lett. 32, 305 (1978).
16. K. Fujiwara, T. Fujiwara, K. Hori, and M. Takusagawa, Appl. Phys. Lett. 34, 668 (1979).
17. R. W. Dixon and W. B. Joyce, IEEE J. Quantum Electron. QE-15, 470 (1979).
18. H. C. Casey, Jr. and E. Buehler, Appl. Phys. Lett. 30, 247 (1977).
19. Semiannual Technical Summaries on Electrooptical Devices, Lincoln Laboratory, M.I.T. (30 September 1977), p. 7, DDC AD-A054477/5; (31 March 1978), p. 3, DDC AD-A059062/0; (30 September 1978), p. 3, DDC AD-A069091/7.
20. C. E. Hurwitz and J. J. Hsieh, Appl. Phys. Lett. 32, 487 (1978), DDC AD-A060752/3.
21. K. Nishida, K. Taguchi, and Y. Matsumoto, Appl. Phys. Lett. 35, 251 (1979).
22. K. Taguchi, Y. Matsumoto, and K. Nishida, Electron. Lett. 15, 483 (1979).
23. J. P. Donnelly and C. E. Hurwitz, Appl. Phys. Lett. 31, 418 (1977), DDC AD-A050856/4; also Semiannual Technical Summary on Electro-optical Devices, Lincoln Laboratory, M.I.T. (30 September 1977), p. 11, DDC AD-A054477/5.
24. D. E. Davies, J. P. Lorenzo, and T. G. Ryan, Solid-State Electron. 21, 981 (1978).
25. J. J. Berenz, F. G. Frank, and T. L. Hierl, Electron. Lett. 14, 683 (1978).
26. J. P. Donnelly and C. E. Hurwitz, Solid-State Electron. 21, 475 (1978), DDC AD-A053929/6; also Semiannual Technical Summary on Electro-optical Devices, Lincoln Laboratory, M.I.T. (30 September 1978), p. 13, DDC AD-A069091/7.

27. W. T. Devlin, K. T. Ip, D. P. Leta, L. F. Eastman, and G. H. Morrison, in Gallium Arsenide and Related Compounds (1978) St. Louis, C. M. Wolfe, Ed. (The Institute of Physics, London, Conf. Ser. 45, 1979), p. 510.

28. J. P. Donnelly and C. A. Armiento, Appl. Phys. Lett. 34, 96 (1979), DDC AD-A069910/8; also Semiannual Technical Summary on Electro-optical Devices, Lincoln Laboratory, M.I.T. (30 September 1978), p. 9, DDC AD-A069091/7.

29. C. A. Armiento, J. P. Donnelly, and S. H. Groves, Appl. Phys. Lett. 34, 229 (1979), DDC AD-A069937/1; also Semiannual Technical Summary on Electrooptical Devices, Lincoln Laboratory, M.I.T. (30 September 1978), p. 13, DDC AD-A069091/7.

30. D. E. Davies, W. D. Potter, and J. P. Lorenzo, J. Electrochem. Soc. 125, 1845 (1978).

31. K. R. Gleason, H. B. Dietrick, R. L. Henry, E. D. Cohen, and M. L. Bark, Appl. Phys. Lett. 32, 578 (1978).

32. K. R. Gleason, H. B. Dietrick, M. L. Bark, and R. L. Henry, Electron. Lett. 14, 643 (1978).

33. D. E. Davies, J. J. Comer, J. P. Lorenzo, and T. G. Ryan, Appl. Phys. Lett. 35, 142 (1979).

34. J. P. Donnelly, C. A. Armiento, V. Diadiuk, and S. H. Groves, Appl. Phys. Lett. 35, 74 (1979), DDC AD-A076746; also Semiannual Technical Summary on Electrooptical Devices, Lincoln Laboratory, M.I.T. (31 March 1979), p. 5, DDC AD-A077152.

35. R. Becker, Solid-State Electron. 16, 1241 (1973).

36. L. J. van der Pauw, Philips Res. Rep. 13, 1 (1958).

37. J. P. Donnelly and C. E. Hurwitz, Solid-State Electron. 20, 727 (1977), DDC AD-A054406/4.

38. J. D. Sansbury and J. F. Gibbons, Radiat. Effect 6, 269 (1970).

39. W. J. Johnson and J. F. Gibbons, Projected Range Statistics in Semiconductors (Stanford University Bookstore, 1970); also J. F. Gibbons, W. T. Johnson, and S. W. Mybroie, Project Range Statistics (Halsted Press, New York, 1975).

40. J. Lindhard, M. Scharff, and H. Schiott, K. Dan. Vidensk. Selsk., Mat.-Fys. Medd. 33, 1 (1963).

41. B. K. Shin, D. C. Look, Y. S. Park, and J. E. Ehret, J. Appl. Phys. 47, 1574 (1976).

42. R. Zolch, H. Ryssel, H. Kranz, H. Reichl, and I. Range, in Ion Implantation in Semiconductors and Other Materials, 1976, F. Chernow et al., Eds. (Plenum, New York, 1977), p. 593.

43. B. K. Shin, Appl. Phys. Lett. 29, 438 (1976).

44. W. Rothemund and C. R. Fritzsche, J. Vac. Sci. Technol. 16, 968 (1979).

45. J. P. Donnelly, in Gallium Arsenide and Related Compounds (St. Louis) 1976, L. F. Eastman, Ed. (The Institute of Physics, London, Conf. Ser. 333, 1977), p. 166, DDC AD-A046986/6.

46. R. L. Moon, G. A. Antypas, and L. W. James, J. Electron. Mater. 3, 635 (1974).

47. J. J. Hsieh, J. Electron. Mater. 7, 31 (1978), DDC AD-A054571/5.

48. R. E. Nahory, M. A. Pollack, W. D. Johnston, Jr., and R. L. Barns, Appl. Phys. Lett. 33, 659 (1978).

49. P. K. Tien and B. I. Miller, Appl. Phys. Lett. 34, 701 (1979).

UNCLASSIFIED

SECURITY CLASSIFICATION OF THIS PAGE *(When Data Entered)*

REPORT DOCUMENTATION PAGE	READ INSTRUCTIONS BEFORE COMPLETING FORM
1. REPORT NUMBER: ESD-TR-79-279	2. GOVT ACCESSION NO.: AD-A084 410
	3. RECIPIENT'S CATALOG NUMBER
4. TITLE *(and Subtitle)*: Electrooptical Devices	5. TYPE OF REPORT & PERIOD COVERED: Semiannual Technical Summary Rept. 1 Apr – 30 Sep 79
	6. PERFORMING ORG. REPORT NUMBER
7. AUTHOR(s): Charles E. Hurwitz	8. CONTRACT OR GRANT NUMBER(s): F19628-80-C-0002
9. PERFORMING ORGANIZATION NAME AND ADDRESS: Lincoln Laboratory, M.I.T. P.O. Box 73 Lexington, MA 02173	10. PROGRAM ELEMENT, PROJECT, TASK AREA & WORK UNIT NUMBERS: Program Element Nos. 62702F and 61102F Project Nos. 2306 and 4600
11. CONTROLLING OFFICE NAME AND ADDRESS: Rome Air Development Center Griffiss AFB, NY 13440	12. REPORT DATE: 30 Sept 1979
	13. NUMBER OF PAGES: 32
14. MONITORING AGENCY NAME & ADDRESS *(if different from Controlling Office)*: Electronic Systems Division Hanscom AFB Bedford, MA 01731	15. SECURITY CLASS. *(of this report)*: Unclassified
	15a. DECLASSIFICATION DOWNGRADING SCHEDULE

16. DISTRIBUTION STATEMENT *(of this Report)*

Approved for public release; distribution unlimited.

(11) 2306, 4600

17. DISTRIBUTION STATEMENT *(of the abstract entered in Block 20, if different from Report)*

18. SUPPLEMENTARY NOTES

None

19. KEY WORDS *(Continue on reverse side if necessary and identify by block number)*

electrooptical devices	proton bombardment	ion implantation
avalanche photodiodes	double-heterostructure	GaInAsP/InP lasers

20. ABSTRACT *(Continue on reverse side if necessary and identify by block number)*

This report covers work carried out with support of the Department of the Air Force during the period 1 April through 30 September 1979. A part of this support was provided by the Rome Air Development Center.

The current objectives of the electrooptical device program are: (1) to perform life tests on GaInAsP/InP double-heterostructure (DH) diode lasers operating in the 1.0- to 1.3-μm wavelength region and analyze the degradation mechanisms, and (2) to fabricate and study avalanche photodiodes of similar composition GaInAsP operating in the same wavelength region.

DD FORM 1 JAN 73 1473 EDITION OF 1 NOV 65 IS OBSOLETE

UNCLASSIFIED

SECURITY CLASSIFICATION OF THIS PAGE *(When Data Entered)*

20. ABSTRACT (Continued)

Self-sustained pulsations in light output, similar to those occurring in Al$_x$Ga$_{1-x}$As lasers, have been studied in GaInAsP DH lasers. In marked contrast to observations for AlGaAs lasers, the rate of incidence of the pulsations is much lower and their occurrence does not appear to be increased by aging. The pulsations appear to be related to defects originating in the growth process or subsequent fabrication procedures.

Substantial increase in avalanche gain and reduction of dark current have been achieved in a modified version of the inverted-mesa GaInAsP/InP avalanche photodiode structure. Dark currents as low as 1.5 nA at half the breakdown voltage and photocurrent gains as high as 700 have been measured.

Implantation of the donors Se, Si, and C and the acceptors Cd, Mg, and Be from room temperature to 200°C has been studied. The sample temperature during implantation is found to have a pronounced effect on the electrical characteristics of the resulting layers. Electron concentrations in excess of 10^{19} cm^{-3} have been achieved.

A vector formulation has been devised to describe quantitatively the change in lattice parameters as a function of composition of the alloy $Ga_xIn_{1-x}As_yP_{1-y}$. The technique has potential use in the further development of lattice-matched $Ga_xIn_{1-x}As_yP_{1-y}$ heterostructure lasers and photodetectors.

The diffusion of Zn and Cd into InP has been investigated in order to make a comparative evaluation of these elements as acceptor diffusants for the fabrication of GaInAsP/InP electrooptical devices. The use of Zn is found to be advantageous because p-n junctions with comparable characteristics can be obtained with lower diffusion temperatures than those required for Cd.